Proceedings of ASME Turbo Expo 2021
Turbomachinery Technical Conference and Exposition
GT2021
June 7-11, 2021, Virtual, Online

GT2021-58341

GRADIENT-FREE OPTIMIZATION IN THERMOACOUSTICS: APPLICATION TO A LOW-ORDER MODEL

Johann Moritz Reumschüssel*[a], Jakob G. R. von Saldern[b], Yiqing Li[c], Christian Oliver Paschereit[a], Alessandro Orchini[a]
[a]Chair of Fluid Dynamics, Technische Universität Berlin, Germany
[b]Laboratory for Flow Instabilities and Dynamics, Technische Universität Berlin, Germany
[c]Center for Turbulence Control, Harbin Institute of Technology, Guangdong, China

ABSTRACT

Machine learning and automatized routines for parameter optimization have experienced a surge in development in the past years, mostly caused by the increasing availability of computing capacity. Gradient-free optimization can avoid cumbersome theoretical studies as input parameters are purely adapted based on output data. As no knowledge about the objective function is provided to the algorithms, this approach might reveal unconventional solutions to complex problems that were out of scope of classical solution strategies. In this study, the potential of these optimization methods on thermoacoustic problems is examined. The optimization algorithms are applied to a generic low-order thermoacoustic can-combustor model with several fuel injectors at different locations. We use three optimization algorithms – the well established Downhill Simplex Method, the recently proposed Explorative Gradient Method, and an evolutionary algorithm – to find optimal fuel distributions across the fuel lines while maintaining the amount of consumed fuel constant. The objective is to have minimal pulsation amplitudes. We compare the results and efficiency of the gradient-free algorithms. Additionally, we employ model-based linear stability analysis to calculate the growth rates of the dominant thermoacoustic modes. This allows us to highlight general and thermoacoustic-specific features of the optimization methods and results. The findings of this study show the potential of gradient-free optimization methods on combustor design for tackling thermoacoustic problems, and motivate further research in this direction.

NOMENCLATURE

$\mathbf{A}_{ac}$	acoustic matrix
$\mathbf{A}_q$	heat release matrix
A_c	duct cross section area
α	mixture weight coefficient
c	speed of sound
DSM	downhill simplex method
EA	evolutionary algorithm
EGM	explorative gradient method
f, g	down-, upstream travelling acoustic wave
F	transport transfer function
FTF	flame transfer function
J	objective function
N	number of injectors
ω	angular frequency
p	pressure
Pe	Péclet number
ϕ	equivalence ratio
q	heat release
R	reflection coefficient
ρ	density
s_t	turbulent flame speed
σ	growth rate
u	velocity

*Address all correspondence to this author, reumschuessel@tu-berlin.de

INTRODUCTION

In modern combustion systems, lean premixed flames are used in order to reduce emission of harmful combustion by-products such as nitrogen oxides. These are however highly sensitive to fluctuations in pressure, flow velocity and gas composition, causing unsteadiness in the flame heat release rate, which in turn acts as an acoustic source. The feedback cycle between the acoustics in the combustion chamber and the flame can cause thermoacoustic instabilities that can severely affect the performance of the equipment and can even lead to mechanical damage [1]. In order to make the flames less susceptible to unsteady phenomena, an increased equivalence ratio – and thus, increased nitrogen oxides production – must be accepted, at least locally. Therefore, a combustor design is always related to the balancing between emissions and pulsations [2].

Detailed simulations or experimental parametric studies aimed at finding suitable operating conditions with low emissions and low pulsations prove to be particularly cost intensive. In practice, this development process is strongly influenced by the experience and intuition of specialized engineers [3]. Reduced order approaches to better understand the effect that parametric variations have on the operation of a combustor, and the retrofitting of this information at the design stage have been an extensive subject of research in the past. Several studies have been conducted on low-order networks, which are based on both physical and empirical information and are able to predict the influence of the system parameters on its stability. These physics and data-based models can be adopted to simulate complex thermoacoustic phenomena like bifurcation and can-to-can interaction [4,5,6,7]. Low-order models can be exploited, e.g., to identify optimal damper configurations for suppressing thermoacoustic oscillations [8], or can be combined with adjoint methods to identify the sensitivity of system eigenvalues to different parameter changes [9].

An alternative approach to find optimal parameters is gradient-free optimization. It treats the system (or parts of it) as an unknown function and tunes the input parameters to minimize a specific objective value, e.g., the amplitude of pressure pulsations, without knowledge of the underlying physical equations. Although the application of gradient-free optimization routines to physical problems does not provide direct physical insights, these methods are very generic, and therefore usable for optimizing problems of very different nature. Gradient-free optimization methods have been applied to combustion systems in the past, mainly focusing on evolutionary methods. Corresponding applications to reduce NO_X emissions and thermoacoustic pulsations by use of automatized experiments were presented in [10] and [11]. Both studies applied evolutionary algorithms, particularly suitable for multi-dimensional objective functions, to optimize the distribution of fuel injection in an industrial gas turbine combustor. Further experimental work was presented in [12], using an evolutionary algorithm to optimize feedback controllers for fuel injection in a scaled gas turbine combustor. Other gradient-free optimization approaches than evolutionary strategies are rare in the field of combustion. In [13], the downhill simplex method (DSM) and an evolutionary algorithm are applied and compared to a CFD model of a laminar flame, reducing CO emissions by fuel distribution.

Well-developed optimization routines, like DSM and evolutionary optimization algorithms, are available in commercial and non-commercial software packages. However, finding faster and more robust algorithms that can handle complex constraints and high-dimensional problems remains an active research topic, especially because of the diversity of potential applications [14,15]. Since no physical model is required, these black-box optimization routines can be equally applied to simulation and experimental data to find optimal input parameters [16,17]. If an appropriate parametrization is prescribed, even closed-loop control laws can be tuned by modern methods [18]. Recent research on gradient-free optimization in fluid mechanics has developed robust methods, which have less chances of remaining trapped in local minima, and higher chances of identifying the global minimum while requiring only a low number of function evaluations [19].

In this study we discuss the applicability of gradient-free optimization algorithms in thermoacoustics, by comparing well-developed and recently published optimization methods. To do so, we consider a generic nonlinear low-order thermoacoustic can-combustor model in time domain. The amplitude of pressure fluctuations at a prescribed location serves as the objective function for the optimization. The model enables a gradual increase of complexity and is able to reproduce typical properties of thermoacoustic systems. It is therefore suited to compare optimization routines, especially with respect to thermoacoustic-specific requirements. The goal of the optimization algorithms is to reduce thermoacoustic pulsations by distributing the injection of a fixed amount of fuel across various axially staged injection lines, without explicit use of the model's equations. For an in-depth understanding of the results found by the gradient-free optimizers, we also exploit our knowledge of the underlying thermoacoustic equations. By linearizing the governing equations, we can investigate the stability of the thermoacoustic system in frequency domain and provide physical insights into the results of the gradient-free optimizers.

The study is structured as follows. First, the nonlinear acoustic and flame models are presented in detail in time domain. For the frequency analysis, the linearization is shown in broad outlines. Second, the gradient-free optimization algorithms are described. Third, the algorithms are applied to the generic thermoacoustic model with the aim of minimizing acoustic pulsations. Lastly, the results are discussed in detail and compared to the linear stability analysis.

THERMOACOUSTIC MODEL

We consider a generic axial combustor as sketched in Fig. 1. The thermoacoustic model is based on plane acoustic waves, which cause fluctuations of equivalence ratio at the fuel injectors. The equivalence ratio fluctuations are convected towards the flame, which responds with heat release fluctuations that in turn generate acoustics. A position x_m downstream of the flame is chosen at which pressure fluctuations are extracted. For the geometry and thermoacoustic frequencies investigated in this study, this reference location is known to not be at a pressure node. The amplitude of the pressure fluctuations at this location will be used as an objective function for the optimization. The coupled thermoacoustic model is integrated in time using Simulink. In the following, each of the components of the model is presented in detail.

Acoustics

The acoustic system is divided into two regions, up- and downstream of the flame, each with uniform mean flow velocity, pressure and temperature, respectively, as shown in Fig. 1. By assuming only plane acoustic waves, the one-dimensional acoustic pressure and velocity in the regions upstream ($l = 1$) and downstream ($l = 2$) of the flame read [5]

$$p_l'(x,t) = \hat{p}_l(x)e^{st} = \left(f_l e^{-\frac{xs}{c_l+\bar{u}_l}} + g_l e^{\frac{xs}{c_l-\bar{u}_l}}\right)e^{st}, \tag{1}$$

$$u_l'(x,t) = \hat{u}_l(x)e^{st} = \frac{1}{\bar{\rho}_l c_l}\Big(\underbrace{f_l e^{-\frac{xs}{c_l+\bar{u}_l}}}_{\hat{f}_l(x)} - \underbrace{g_l e^{\frac{xs}{c_l-\bar{u}_l}}}_{\hat{g}_l(x)}\Big)e^{st}, \tag{2}$$

where $s \equiv \sigma + i\omega$ denotes the complex frequency, c_l is the speed of sound, $\bar{u}_l$ is the mean flow velocity and g_l and f_l are the amplitudes of the up- and downstream travelling acoustic waves. Entropy waves are neglected, which yields the isentropic relation $\rho_l' = p_l'/c_l$. The flame is assumed to be compact and the heat release is modelled at a steady position x_f as a discontinuity. By applying mass, momentum and energy conservation laws the flame element can be incorporated into the model via the Rankine-Hugoniot jump conditions [5]

$$\rho_1 u_1 = \rho_2 u_2, \tag{3}$$

$$p_1 + \rho_1 u_1^2 = p_2 + \rho_2 u_2^2, \tag{4}$$

$$\rho_2 u_2 \left[\frac{\gamma}{(\gamma-1)}\frac{p_2}{\rho_2} + \frac{u_2^2}{2}\right] = \frac{q}{A_c} + \rho_1 u_1 \left[\frac{\gamma}{(\gamma-1)}\frac{p_1}{\rho_1} + \frac{u_1^2}{2}\right], \tag{5}$$

where q is the heat release rate of the flame, γ is the ratio of specific heats, and A_c denotes the cross-sectional area of the combustor. By linearizing Eqs. (3)-(5) and choosing a harmonic ansatz for the fluctuating quantities $z' = \hat{z}e^{st}$, $(z = p, q, \rho, u)$ the jump conditions can be embedded into the model in terms of acoustic waves. At the up- and downstream end of the domain, the acoustic model is closed by means of reflection coefficients R_1 and R_2. The linear acoustic model is incorporated into Simulink with a wave-based approach using time-lag blocks.

Equivalence Ratio Fluctuations

Upstream of the flame, at the positions of the fuel injectors, the acoustic oscillations cause fluctuations of the equivalence ratio. We assume N stiff fuel injectors, meaning that the injection system is acoustically fully decoupled from the duct. This assumption implies that the fuel mass flow rate is not affected by acoustic fluctuations, whereas the air mass flow rate fluctuates according to the unsteady velocity at the corresponding injection position x_k. Since the transport of the equivalence ratio is a linear process, we decompose its convection and diffusion into components $\phi_k'(x)$. Each ϕ_k' is the contribution to the total equivalence ratio fluctuation that has been caused by acoustic unsteadiness at the injector k. Then, the arising equivalence ratio fluctuations at injector position $\phi_k'(x_k)$ can be found as a function of the corresponding velocity fluctuations $u'(x_k)$ as [20]

$$\frac{\phi_k'(x_k)}{\bar{\phi}} = -\frac{u'(x_k)}{\bar{u}_1 + u'(x_k)}. \tag{6}$$

The transport of the equivalence ratio fluctuation from each of the injection positions towards the flame is modelled as a diffusion-convection process

$$(\partial_t + \bar{u}_1\partial_x - \Gamma\partial_x^2)\phi_k' = 0, \tag{7}$$

where ∂_t and ∂_x denote time and spatial derivatives, respectively, and Γ is the effective diffusion coefficient. The advection velocity is assumed to be constant and equal to the mean flow in the upstream part of the duct, $\bar{u}_1$. We then superpose the individual components to obtain the total equivalence ratio at any location:

$$\phi(x) = \bar{\phi} + \sum_{k=1}^{N} \alpha_k \phi_k'(x). \tag{8}$$

The mechanism is also illustrated in Fig. 1. In Eq. (8), α_k are mixing weights that quantify how much fuel has been injected at location x_k. We assume that each α_k can continuously span between 0 (injection line valve fully closed) and 1 (injection line valve fully opened). By varying the mixing weights, one can vary the axial fuel distribution through the injectors, which affects the flame behavior and in turn the thermoacoustic stability. In the following, we shall assume that the total amount of fuel injected into the system cannot be varied. This restriction on the total fuel

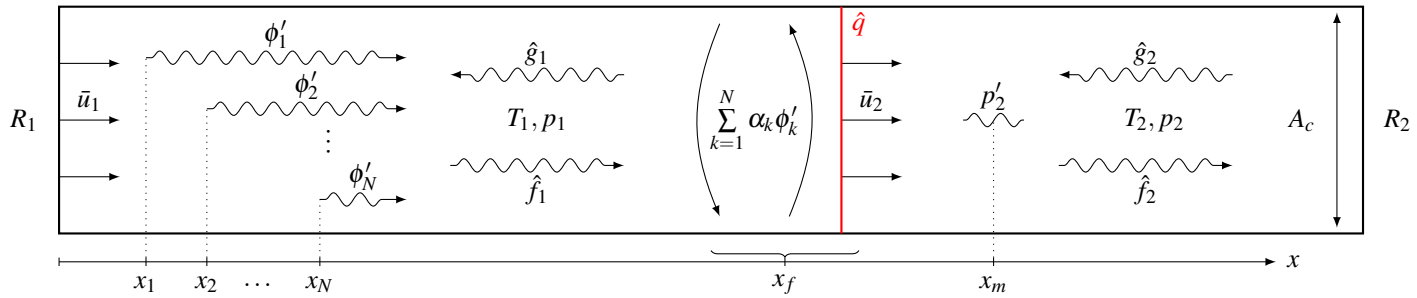

FIGURE 1. One-dimensional model of acoustics and equivalence ratio fluctuation transport. The system is divided into an upstream and a downstream region, each with uniform mean velocity, mean pressure and temperature. Fuel injectors are marked with x_1 to x_N, the superposition is indicated at the flame location x_f and pressure oscillations for the objective function are taken at location x_m.

mass flow imposes a constraint on the mixing weights α_k, which we express as:

$$\sum_{k=1}^{N} \alpha_k = 1. \tag{9}$$

By casting the ϕ-fluctuations in frequency domain, a transfer function between fluctuations at injection position x_k and the flame location x_f can be derived from Eq. (7),

$$F_k(s) = \frac{\hat{\phi}_k(s,x_f)}{\hat{\phi}_k(s,x_k)} = \exp\left[\frac{\mathrm{Pe}_k}{2}\left(1-\sqrt{1+4s\tau_k\mathrm{Pe}_k^{-1}}\right)\right], \tag{10}$$

where $\tau_k \equiv L_k/\bar{u}_1$ is a characteristic convection time, $\mathrm{Pe}_k \equiv \bar{u}_1 L_k/\Gamma$ is the Péclet number, the ratio of convective and diffusive time scale and L_k is the transport length from injector k to the flame [4]. To allow for an implementation in the time domain model, each transfer function F_k is approximated by a first order ODE-system, relating equivalence ratio fluctuations at the injector and at the flame, expressed in the form of a linear state-space model [21]:

$$\dot{\mathbf{z}}_k = \mathbf{A}_k\mathbf{z}_k + \mathbf{b}_k\phi_k'(t,x_k), \quad \phi_k'(t,x_f) = \mathbf{c}_k^{\mathrm{T}}\mathbf{z}_k. \tag{11}$$

The matrices $\mathbf{A}_k$ and vectors $\mathbf{b}_k$, $\mathbf{c}_k$ are obtained by fitting the frequency response of Eq. (11) within an appropriate frequency range [22], and $\mathbf{z}_k$ is an auxiliary state vector. Finally, at the flame location x_f, the total equivalence ratio fluctuations are calculated by combining Eqs. (8) and (10):

$$\hat{\phi}(s,x_f) = \sum_{k=1}^{N} \alpha_k F_k(s)\hat{\phi}_k(s,x_k). \tag{12}$$

An analogous expression can be found in time domain by using the state-space formulation (11).

Flame model

It is assumed that equivalence ratio fluctuations are the dominant phenomenon driving the heat release rate fluctuations. Further coupling mechanisms between the acoustics and heat release are neglected. This assumption has already been employed in similar models in the literature that also showed qualitative agreement with measurement data [4] and is not restrictive for the purposes of this study. The unsteady heat release is calculated via [1]

$$q(t) = \bar{\rho}_1 A_c s_t(t) h_R(t), \tag{13}$$

where s_t is the turbulent flame velocity, h_R the reaction enthalpy, $\bar{\rho}_1$ the mean upstream density, and we have assumed that the flame surface area equals the cross section of the duct, A_c. The heat release rate implicitly depends on the equivalence ratio via the turbulent flame speed and the reaction enthalpy. The turbulent flame speed dependency on the mixture ϕ is modelled with an empirical law that reads [4, 23, 24]

$$s_t = s_l\left[1+C\left(\frac{V}{s_l}\right)^n\right], \qquad s_l = a\phi^b e^{-c(\phi-d)^2}. \tag{14}$$

In the above equations, s_l is the laminar flame speed. We shall assume in the following that the mean equivalence ratio is $\bar{\phi} = 0.6$. The remaining coefficients are empirical constants available in the literature for methane-air flames at atmospheric conditions and are reported in Appendix A. For the dependency of the reaction enthalpy on the fuel-air mixture we adopt the following relation [25],

$$h_R = 2.9125\times10^6 \frac{\min(\phi,1)}{1+0.05825\phi}\frac{\mathrm{J}}{\mathrm{kg}}. \tag{15}$$

The flame model is complemented with a symmetrical saturation function, that limits heat release fluctuations $q'(t) = q(t) - \bar{q}$ to

10% of the mean heat release. A noise term is additionally included in the flame model in the form of a normally distributed random number generator, producing heat release fluctuations with a variance of 1 % of the mean heat release $\bar{q}$. By feeding the heat release rate fluctuations into the acoustics, via the Rankine-Hugoniot jump conditions, Eqs. (3) to (5), the thermoacoustic feedback loop is closed. We highlight that the model contains nonlinear dependencies: the relation between the mixture and the acoustic fluctuations, Eq. (6), and the heat release rate response model, Eqs. (13) to (15) plus the static saturation. These nonlinearities are responsible for the saturation of thermoacoustic instabilities to finite amplitude oscillations, that we wish to quantify.

FREQUENCY ANALYSIS

The optimization routines that will be applied in time domain are model-free. No information on the equations will be used by the optimizer. Nonetheless, physical knowledge can aid in understanding the routes taken by the optimization algorithms, and in comparing and interpreting their results. Therefore, in this section we discuss the linear stability analysis of the system in frequency domain, which uses explicit knowledge of the governing equations. By decomposing the acoustics in the cold and hot section of the duct into the Riemann invariants f and g and by linearizing the jump conditions, the (linear) acoustics can be written as

$$\mathbf{A}_{ac}(s) \underbrace{\begin{bmatrix} g_1 \\ f_1 \\ g_2 \\ f_2 \end{bmatrix}}_{=:\mathbf{g}} = \begin{bmatrix} 0 \\ 0 \\ \frac{\hat{q}}{c_1 A_c} \\ 0 \end{bmatrix}, \tag{16}$$

where $\mathbf{A}_{ac}(s)$ is the frequency dependent acoustic matrix, as it can be found e.g. in [5, 21]. By setting $\hat{q} = 0$ the thermoacoustic system reduces to a purely acoustic system, whose eigenmodes are governed by the matrix operator $\mathbf{A}_{ac}(s)$. For an analysis of the full thermoacoustic system, the fluctuating heat release is expressed in frequency domain by means of the flame transfer function (FTF) approach [26]. Equations (6) to (15), which represent the generation of equivalence ratio fluctuations, their transport and their coupling with the flame, are linearized and combined to express the heat release fluctuations in terms of the acoustic velocity fluctuations at the injection locations

$$\hat{q} = \sum_k \mathrm{FTF}_k(s)\, \hat{u}(x_k). \tag{17}$$

Each $\mathrm{FTF}_k(s)$ describes the heat release rate response to velocity fluctuations at the injector position x_k. They depend on the mean field quantities and the model parameters. Their frequency dependency originates from the transport term – see Eq. (10). Lastly, the heat release fluctuations can be expressed in terms of the f and g invariants. The linear equations of the full thermoacoustic system can then be written as

$$\left[\mathbf{A}_{ac}(s) + \mathbf{A}_q(s)\right]\, \mathbf{g} = \mathbf{0}, \tag{18}$$

where $\hat{q}$ was casted into $\mathbf{A}_q(s)$ through Eqs. (2) and (17). The eigenvalues of Eq. (18) represent growth rates and frequencies of thermoacoustic modes. To benchmark the time and frequency domain implementations, growth rates and frequencies were also extracted from transient time domain simulation data. The frequencies were extracted by means of a Fast Fourier Transform and the growth rates were extracted by means of a linear fit onto the transient evolution of the pressure oscillations amplitudes in logarithmic scale [27]. These were in very good agreement (not shown) with the corresponding eigenvalues of Eq. (18), validating the numerical implementations.

PROBLEM FORMULATION

In order to run the optimization, the low-order model, representing the physical system in time domain is treated as an unknown function by the optimization routines. No information on the governing equations is used to find optimal operating conditions, only the values that the input parameters and the cost function take are used. The input parameters are the fuel weights α_k, introduced in Eq. (8). Due to the constraint on the sum of weights, Eq. (9), the problem dimension equals the number of injectors minus one. The cost function is the root mean square (RMS) of the pressure fluctuations at a reference location at steady state conditions. Convergence to steady state oscillations was assumed to have been reached after a simulation time of 5 s. The pulsation amplitude RMS is calculated on the fly as a running average over a specified time interval, $T_{RMS} = 1$ s. The goal of the optimization algorithms is to find the optimal fuel distribution, such that the pulsation at the reference location x_m is minimized subject to appropriate constraints on the parameters. By indicating with $\boldsymbol{\alpha} \equiv [\alpha_1, \ldots, \alpha_N]$ the whole set of considered fuel weights, the optimization problem formally reads:

$$\arg\min_{\boldsymbol{\alpha}} J(\boldsymbol{\alpha}), \tag{19a}$$

$$\text{subject to } \left\{ \boldsymbol{\alpha} \mid 0 \le \alpha_k \le 1 \wedge \sum_{k=1}^{N} \alpha_k = 1 \right\}, \tag{19b}$$

$$\text{with } J(\boldsymbol{\alpha}) = \frac{1}{T_{RMS}} \left[\int_{T_{RMS}} \left[p'(x_m, t; \boldsymbol{\alpha}) \right]^2 \mathrm{d}t \right]^{1/2}. \tag{19c}$$

OPTIMIZATION ROUTINES

In this section, we compare different optimization methods to solve (19) that are briefly presented in this section. The methods all seek to find the global minimum of $J(\boldsymbol{\alpha})$ as per Eq. (19a) within the entire parameter space defined by (19b) by testing different values of $\boldsymbol{\alpha}$. In the following, each input parameter combination $\boldsymbol{\alpha}_n$ is referred to as a point in parameter space. The values of the optimization parameters can be found in Appendix A.

Downhill Simplex Method. The exploitive Downhill Simplex Method (DSM) [15] is a well-known method to find local minima by iteratively comparing values of the objective function $J(\boldsymbol{\alpha})$ of a group of $P+1$ points, referred to as a simplex $\mathscr{S} \equiv \{\boldsymbol{\alpha}_1, \boldsymbol{\alpha}_2, \ldots, \boldsymbol{\alpha}_{P+1}\}$, where P is the number of parameters to optimize. As emphasized above, the number of input parameters P for the problem regarded here equals $N-1$, where N is the number of fuel injectors and the minus one originates from the constraint in Eq. (9). The method is sketched in Alg 2.

Explorative Gradient Method. The Explorative Gradient Method (EGM) [19] is a recently proposed algorithm that combines the DSM with Latin Hypercube Sampling (LHS), an effective way to explore the parameter space [28]. In EGM, DSM steps are alternated with LHS steps to explore arbitrarily constrained parameter spaces, aiming to increase the chances of finding the set of parameters $\boldsymbol{\alpha}$ at which the objective function has a global minimum. The algorithm is outlined in Alg. 1.

Evolutionary Algorithm. Evolutionary algorithms are optimization routines inspired by biological evolution mechanisms and represent a wide field of research. A number of combinations of input parameters $\mathscr{G} \equiv \{\boldsymbol{\alpha}_1, \boldsymbol{\alpha}_2, \ldots, \boldsymbol{\alpha}_M\}$, referred to as individuals, form a generation. According to their function value $J(\boldsymbol{\alpha}_j)$, the individuals of a generation are modified, combined or transferred to the next generation. In this study we use the algorithm proposed in [29]. Each generation consists of $M = 30$ individuals, where the individuals are N-dimensional arrays of continuous numbers between 0 and 1, representing the mixing weights α_k. In each generation, the best 15 individuals are intermixed in pairs (recombination) and the resulting parameter combinations (descendants) are randomly modified (mutation). The best individual is directly copied to the next generation (elitism). Additionally, an extension for self-optimization of the mutation rate as presented in [30] was included and a χ^2-test was used as a stopping criterion as it is discussed in [31]. Further details on the method can be found in the literature.

RESULTS

To investigate the model features, the characteristics of the optimization algorithms and their performance, different scenarios in increasing order of complexity are analyzed in the following. They differ in terms of the number of fuel injectors, their positions as well as the flame position and the reflection coefficients.

Algorithm 1: Explorative Gradient Method

Initialization: Generate Simplex $\mathscr{S}$ as a set of N points.

Preallocation: All simulated points will be stored in database $\mathscr{B}$.

Discretization: Create a set of points $\mathscr{H}$, spanning the constrained parameter space with equal spacing.

while $\sqrt{\frac{1}{N-1}\sum_{j=1}^{N}(J(\boldsymbol{\alpha}_j) - J(\bar{\boldsymbol{\alpha}}))^2} > \delta$ **do**

$(\mathscr{S}, \mathscr{B}) \leftarrow \mathtt{DSM}(\mathscr{S})$

$(\mathscr{S}, \mathscr{B}) \leftarrow \mathtt{LHS}(\mathscr{S}, \mathscr{B}, \mathscr{H})$

Case I. As an exemplary case, we start considering a constrained problem with $N = 2$ fuel injectors at fixed locations. The constraint on the mixing weights (9) makes so that only one of the mixing weights, α_1, is an independent degree of freedom (dof), whereas $\alpha_2 = 1 - \alpha_1$. The chosen system parameters for this case can be found in Tab. 4 of Appendix A. Figure 2 shows the trajectory of the two dominant eigenvalues, resulting from variations in α_1, obtained by solving the linearized equations (18). Two eigenvalues are found in the vicinity of the stability margin, one around 100 Hz and one around 300 Hz. All other identified eigenfrequencies have a very large negative growth rate. Because of this they do not participate in the dynamics and are not shown here. If the fuel is only injected through the downstream injector i.e. $\alpha_1 = 0$, the mode at 300 Hz is unstable with a growth rate of around 19 s^{-1} while the mode at 100 Hz is stable. When shifting the fuel distribution towards the upstream injector, the growth

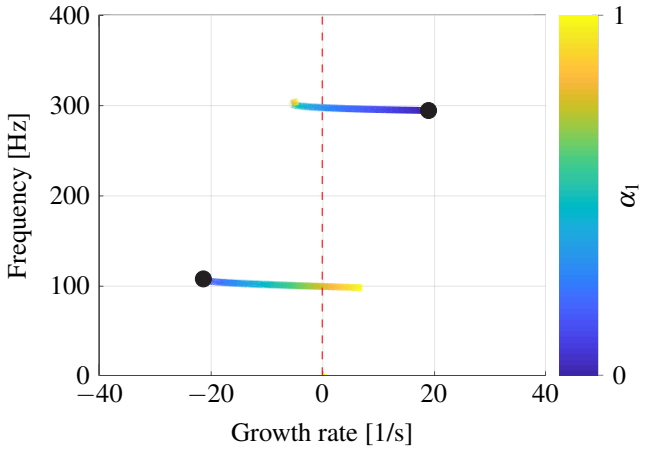

FIGURE 2. Variation of eigenvalues with changing mixing weight α_1. Red dashed line represents stability margin. Circles show eigenvalues for $\alpha_1 = 0$

Algorithm 2: Downhill Simplex Method and Latin Hypercube Sampling

Function DSM($\mathscr{S}$):

Ordering:
Sort and label $\mathscr{S} = \{\boldsymbol{\alpha}_1, \boldsymbol{\alpha}_2, \ldots \boldsymbol{\alpha}_N\}$ by cost such that $J(\boldsymbol{\alpha}_1) \leq J(\boldsymbol{\alpha}_2) \leq \ldots \leq J(\boldsymbol{\alpha}_N)$.
Centroid:
Compute the centroid of the $N-1$ best points, $\bar{\boldsymbol{\alpha}} = \frac{1}{N-1} \sum_{j=1}^{N-1} \boldsymbol{\alpha}_j$.
Reflection:
Reflect the worst vertex towards the best side, $\boldsymbol{\alpha}_r = \bar{\boldsymbol{\alpha}} + (\bar{\boldsymbol{\alpha}} - \boldsymbol{\alpha}_N)$.
if $J(\boldsymbol{\alpha}_1) \leq J(\boldsymbol{\alpha}_r) \leq J(\boldsymbol{\alpha}_{N-1})$ **then**
  Replace $\boldsymbol{\alpha}_N$ by $\boldsymbol{\alpha}_r$.
else if $J(\boldsymbol{\alpha}_r) < J(\boldsymbol{\alpha}_1)$ **then**
  Expansion:
  Expand further in this direction by a factor 2, $\boldsymbol{\alpha}_e = \bar{\boldsymbol{\alpha}} + 2(\bar{\boldsymbol{\alpha}} - \boldsymbol{\alpha}_N)$.
  Replace $\boldsymbol{\alpha}_N$ by the best point of $\boldsymbol{\alpha}_r$ and $\boldsymbol{\alpha}_e$.
else
  if $J(\boldsymbol{\alpha}_r) < J(\boldsymbol{\alpha}_N)$ **then**
    Replace $\boldsymbol{\alpha}_N$ by $\boldsymbol{\alpha}_r$.
  end
  Contraction:
  Contract the worst vertex towards the centroid, $\boldsymbol{\alpha}_c = \bar{\boldsymbol{\alpha}} + \frac{1}{2}(\boldsymbol{\alpha}_N - \bar{\boldsymbol{\alpha}})$.
  if $J(\boldsymbol{\alpha}_c) \leq J(\boldsymbol{\alpha}_N)$ **then**
    Replace $\boldsymbol{\alpha}_N$ by $\boldsymbol{\alpha}_c$.
  else
    Shrink: Shrink the simplex, $\boldsymbol{\alpha}_i \mapsto \boldsymbol{\alpha}_1 + \frac{1}{2}(\boldsymbol{\alpha}_i - \boldsymbol{\alpha}_1), i = 2, \ldots, N$.
  end
end
Update Simplex: $\mathscr{S} = \{\boldsymbol{\alpha}_1, \boldsymbol{\alpha}_2, \ldots, \boldsymbol{\alpha}_N\}$
Update Database: Add all newly evaluated Points to database $\mathscr{B}$.
return

Function LHS($\mathscr{S}, \mathscr{B}, \mathscr{H}$):

Exploration: Select $\boldsymbol{\alpha}_{LHS}$ from $\mathscr{H}$, such that $\boldsymbol{\alpha}_{LHS} = \arg\max_{\boldsymbol{\alpha} \in \mathscr{H}} \min_{\boldsymbol{\alpha}_h \in \mathscr{B}} \|\boldsymbol{\alpha} - \boldsymbol{\alpha}_h\|$
if $J(\boldsymbol{\alpha}_{LHS}) \leq J(\boldsymbol{\alpha}_N)$ **then**
  Replace $\boldsymbol{\alpha}_N$ by $\boldsymbol{\alpha}_{LHS}$
end
Update Simplex: $\mathscr{S} = \{\boldsymbol{\alpha}_1, \boldsymbol{\alpha}_2, \ldots, \boldsymbol{\alpha}_N\}$
Update Database: Add the newly evaluated point $\boldsymbol{\alpha}_{LHS}$ to database $\mathscr{B}$.
return

TABLE 1. Steps taken by the EGM algorithm for Case I.

α_1	0, 0.25	0.25,0.5	0.5, 1	0.5, 0.75	0.5, 0.625
Step	Initialize	Expand	LHS	Contract	Contract

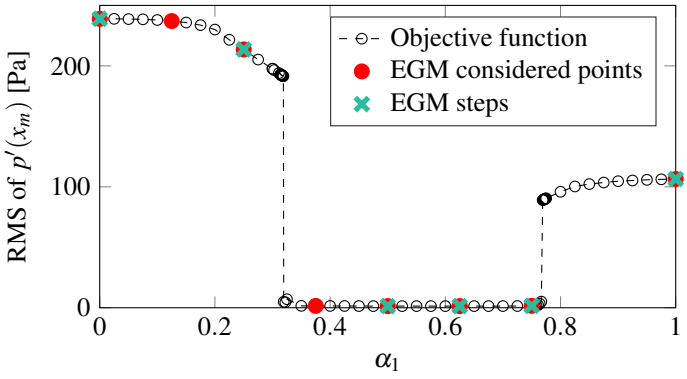

FIGURE 3. Pressure oscillation for variation of mixing weight 1 for the case of two injectors and optimization pathway. Red dots indicate all simulated points by EGM, green dots show actually taken steps.

rate of the 300 Hz mode decreases and it becomes stable, while the low-frequency eigenvalue moves from the stable to the unstable half-plane. For a range of values of α_1 both modes have a negative growth rate. When the fuel is entirely injected through the upstream injector (α_1 = 1), the 100 Hz mode's growth rate is positive and reaches a maximum of 7 s^{-1}, while the mode at 300 Hz is stable.

Before applying the optimization routines, the parameter space was explored by performing time domain simulations over an equidistant grid with step $\Delta\alpha_1 = 0.025$. Corresponding root mean square values of the pressure oscillations from time domain simulations are shown in Fig. 3 (black dots). Near the α values where the eigenvalues cross the stability line, additional simulations were performed. These were simulated for 100 s, as the growth rates are very small in this region.

Information about the stability of the system can equally be drawn from time and frequency domain analysis. For values of mixing weight α_1 between 0.319 and 0.767, where both eigenvalues have negative growth rates, the system is stable. In time domain it shows pressure oscillations lower than 5 Pa, that can be associated with the noise introduced in the flame function. The sudden increase of pressure oscillation amplitude when the eigenvalues become unstable indicates that the thermoacoustic system has undergone subcritical bifurcations. Different types of bifurcations are typical for thermoacoustic systems and potentially place great demands on optimization routines. Indeed, bi-stable areas surely exist for α close to 0.319 and 0.767 in Fig. 3, and one may be interested in identifying the location of fold points to have more information on robustness of stability margins. For this, more simulations or experiments need to be

performed starting from different initial conditions, to explore possible different saturated states. As already stated, however, in the present study all simulations are initialized in stationary state to avoid this additional degree of complexity.

When applied to this one-dimensional case, the EGM optimization algorithm identifies a minimum at $\alpha_1 = 0.625$ after only eight function evaluations by the optimizer. Figure 3 shows all the operations performed by the EGM method until convergence. For each iteration, the regarded set of two points is also indicated in Tab. 1, including the optimization subroutines they originate from. The first DSM expansion step lets the optimizer approach the valley in the first iteration. An explorative LHS step is then performed, inducing a test at the upper boundary $\alpha_1 = 1$. The next two DSM steps leads to convergence in the valley, as the intermediate explorative steps did not indicate any potential improvements.

Case II. Practically, it may not always be possible to change the parameters of a thermoacoustic system to ensure its linear stability. This is the scenario we consider in our second example. To guarantee that the two dominant thermoacoustic modes cannot be simultaneously stabilized by varying the fuel distribution, the downstream reflection coefficient was increased to achieve a lower acoustic damping at the boundary, and the positions of the flame and the fuel injectors were adjusted. Additionally, to increase the dimension of the parameter space, a third fuel injector was added to the setup. The parameters used for this case are listed in Tab. 4 of Appendix A. Although the number of dofs remains limited, it is sufficient to emphasize the challenges encountered when optimizing high-dimensional parameter spaces in conjunction with the complex behaviour of thermoacoustic systems. In fact, thermoacoustic systems can feature many unstable modes – typical examples are clusters in can-annular systems, but also annular or single systems can display multiple thermoacoustic modes that are unstable at the same time [7, 32]. This causes extra challenges since one can expect many local minima, each associated to a certain unstable mode or combinations/groups of modes being suppressed or strongly attenuated.

Before applying the optimization routines, the parameter space was explored by performing time simulation over an equidistant grid with step size $\Delta\alpha_k = 0.01$, to gain insight into the objective function's shape within the parameter space. The RMS pulsation amplitudes can be seen in Figure 4, and will serve as a reference for the following discussion. Note that α_3 is not shown, since it is determined by the constraint (9) and thus is not a dof. In order to further analyze the results, the frequency of the dominant unstable mode in the saturated state is determined in each grid point. It is identified as the frequency with the highest amplitude in the spectrum of the pressure signal, considering the last second of the simulation. Note that, when multiple modes are simultaneously unstable, it is not necessarily the mode with the largest growth rate that dominates the nonlinear

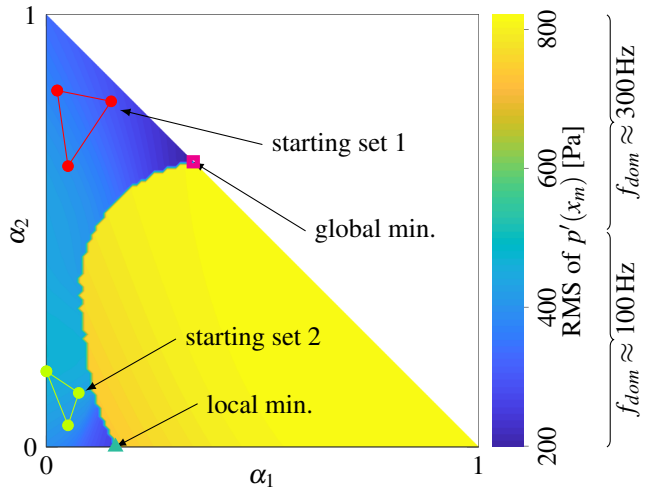

FIGURE 4. Pressure oscillations for variation of fuel distribution for Case II and dominant frequencies, detected from the spectrum of the pressure signal in the saturated state. The objective function features a local and a global minimum. Triangles show sets of starting points as described in the text.

dynamics [7, 32]. It can be seen that the parameter space can be separated into two regions: one in which a 100 Hz oscillation with lower amplitude and one in which a 300 Hz oscillation with higher amplitude dominate the dynamics. In the following, we will refer to these oscillations as Mode 1 and Mode 2, respectively. The pressure fluctuations saturate at higher amplitudes when Mode 1 dominates the spectrum. The system features two minima: a local minimum at $\boldsymbol{\alpha} = [0.15, 0, 0.85]$ and a global minimum at $\boldsymbol{\alpha} = [0.325, 0.675, 0]$. Both minima lie in the region where Mode 1 dominates the dynamics, but are close to the transition to dominance of Mode 2. Figure 5 shows the two dominant thermoacoustic eigenvalues found for the $\boldsymbol{\alpha}$-values at the two minima. On each of the minima, the two growth rates have comparable values, with the high-frequency mode having a slightly greater growth rate than that of the low-frequency mode – despite it is the low-frequency mode that dominates the dynamics. Additionally, the growth rates of the global minimum are larger than those of the local minimum. Thus, in the case at hand, an optimization based on a linear analysis would not be able to identify the operating conditions with the smallest oscillation amplitude. This highlights that growth rates cannot generally be used as indicators for the saturation amplitude of mode shapes. Information on the nonlinear saturation mechanisms are needed, which are best investigated in time domain.

To compare different gradient-free optimization approaches, the well-established DSM is first applied to the two-dimensional problem. The analysis shows that finding a minimum by use of this optimizer is generally possible. However, due to the objective function's shape, this algorithm has a strong tendency to con-

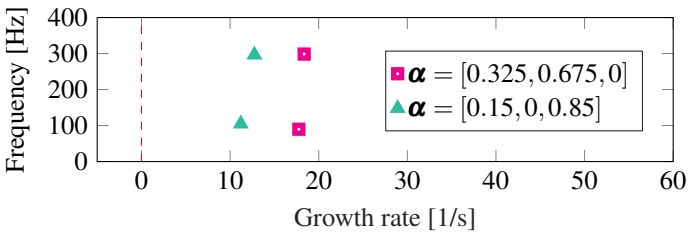

FIGURE 5. Thermoacoustic eigenvalues for the global and local minimum indicated in Fig. 4. Red (green) markers indicate the eigenvalues corresponding to a global (local) minimum of the pressure pulsation amplitude. Notably, the growth rates of the global minimum are larger than those of the local one.

verge to local minima. For some initial conditions, the DSM algorithm correctly finds the global minimum. For example, when starting from the set marked in red in Fig. 4, the DSM requires 209 steps to converge into the global minimum. On the other hand, for initial conditions that do not lie in the valley of the global minimum, the algorithm – which follows the descend of the objective function – will generally converge to a local minimum. For example, when starting from the set marked in green in Fig. 4, the algorithm converges to the nearby sub-optimal local minimum. Despite DSM is a quick and simple algorithm, its tendency to converge to local minima requires the investigation of several initial conditions, which is problematic. When minimization of complexly shaped objective functions is needed, evolutionary algorithms tend to perform well, and we shall now shift the focus on them.

An evolutionary algorithm (EA) with 30 individuals per generation is applied to the problem. As described above, the optimization method features one elitism object, whereas half of the remaining individuals undergo recombination and random-based mutation. Thereby, with enough iterations, the EA explores the parameter space more thoroughly than DSM, and is generally able to find the global minimum. This robust exploration works at the cost of a larger number of evaluated points. To find the global minimum of the thermoacoustic objective function in Fig. 4 within the prescribed tolerance, the evolutionary algorithm needs to run for 48 generations, and thus evaluates a total of 1440 different sets of parameters. The results from the EA optimization are summarized in Fig. 6a. A direct comparison of different optimization methods in terms of required function evaluations only allows limited conclusions to be drawn, since different algorithms have different advantages and convergence properties. However, by looking at Fig. 6a, it is evident that the EA lacks a procedure to effectively follow a gradient, which would speed up convergence once a valley has been identified. Despite the majority of points is generated within the further vicinity of the global minimum, the random-based algorithm requires a relatively high number of function evaluations in this region to identify the minimum and detect convergence.

Lastly, we apply the EGM algorithm to the thermoacoustic problem. Even when starting in the vicinity of a local minimum at starting set 2 (see Fig. 4), the algorithm finds the global minimum after evaluating 363 points. All points that were considered by EGM, starting from starting set 2 are indicated in Fig. 6b. Initially, the DSM steps consider points close to the starting set approaching the local minimum, while the alternated LHS steps explore the parameter space uniformly, increasing spatial resolution in each iteration. Once the LHS sub-routine finds a set of parameters close to the global minimum, the DSM shifts its area of activity towards this region, which has lower objective function values. After some more iterations localized in this part of the parameter space, the DSM algorithm has converged to the global minimum and, since the LHS steps have not identified any better valley, the algorithm stops.

The LHS steps that are performed during the EGM provide for a uniform scanning of the parameter space – a strategy similar to that of the EA; the DSM steps, on the other hand enable effective descending within promising valleys. The shift of focus from one valley to another is triggered by the LHS identification of a single combination of parameters on a structured grid for which the objective function value is smaller than the one of the points considered so far. A drawback is that, if the DSM subroutine is already close to a local-minimum, it may be unlikely to find a set of input parameters that perform better on a structured grid. This would require a very fine exploration (and thus many function calls) or could result in a sub-optimal convergence at a local minimum. In contrast, the EA performs mutation steps in several valleys simultaneously and a risk of such a scenario is hence lower. This advantage is balanced out with slow speed within the valleys.

Case III. To emphasize the possibility of minimizing high-dimensional problems, we finally apply the EGM routine to a configuration with 5 injectors and thus 4 dofs. The geometric and boundary parameters of Case II were maintained, and the system was extended with two additional fuel injectors, in between the previously used ones. The resulting system parameters can be found in Tab. 4 of Appendix A.

In Fig. 7 the current minimum in each iteration is shown. Note that, each iteration consists of a DSM and a LHS step, replacing at least one point of the set. However, only in very few iterations (5,10,17,20,32), this leads to the identification of a new minimum. This new minimum is due to either a LHS or DSM step, indicated respectively with crosses and filled circles in Fig. 7. All the sets of input parameters with which the EGM optimizer has been initialized lead to thermoacoustic instabilities. After 5 iterations, a new optimal set of input parameters is found by LHS, outside the simplex spanned by the starting set. In the next iterations (6-10), further exploration is done by alternating LHS and DSM, eventually leading to identification of a minimum where pressure oscillations of less than 5 Pa are de-

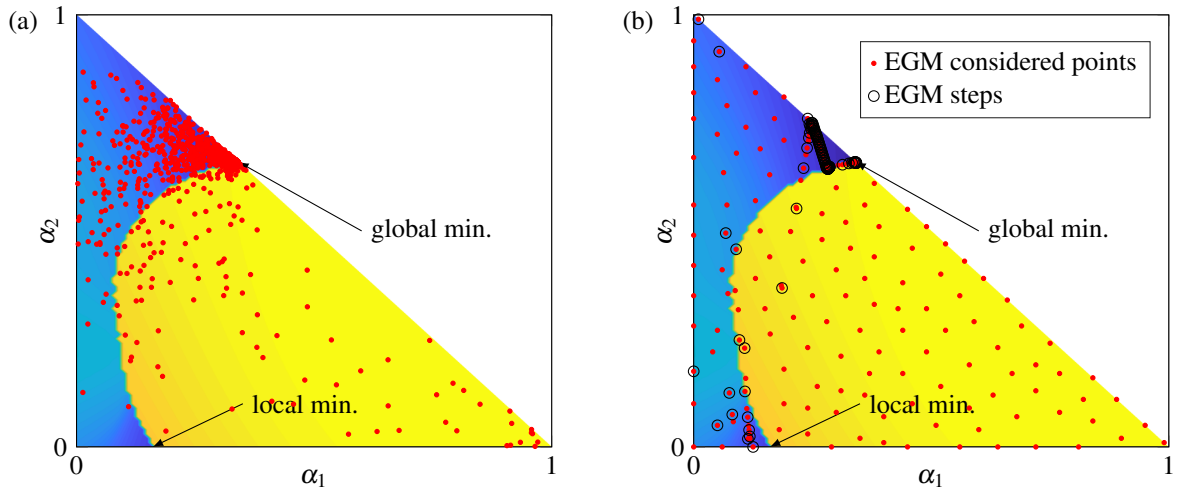

FIGURE 6. Conditions explored by the EA (a) and the EGM (b) for Case II, indicated with red points in the parameter space. Both methods are able to converge to the global minimum. For the EA, once the global minimum valley has been identified, elitism ensures that it will be thoroughly explored to identify with precision the optimal input parameters. For the EGM, black circles show the steps actually taken by optimizer: once a valley is identified, gradient-based information is exploited, which converge to the global minimum more efficiently.

tected. In the remaining iterations, further steps are performed despite the minimal pressure oscillations – which are related to noise – are already small. However, as the stopping criterion considers the objective function values of all the input parameters in the currently considered set, these further steps are required for convergence, which is reached after 35 iterations. To conclude, we recall that the case at hand is an extension of Case II, that always displayed oscillation amplitudes larger than 200 Pa. Hence, Case III demonstrates that the addition of two fuel injectors allows for the stabilization of the system, and that EGM is able to identify a minimum in only 10 iterations – discarding the minor improvements due to the effect of noise.

CONCLUSION

In the present work we investigated the application of various gradient-free optimization algorithms to a generic low-order model of a thermoacoustic can-combustor system with the goal to minimize pressure pulsation amplitudes. The model features multiple fuel injectors and was shown to exhibit thermoacoustic instabilities at multiple frequencies. The optimizers treat the system as a black-box. Their goal is to identify the ideal distribution of fuel across the different injection lines that minimizes the RMS amplitude of the pressure signal extracted downstream of the flame.

We investigated three optimization algorithms, the Downhill Simplex Method (DSM), an evolutionary algorithm (EA), and a recently proposed method that combines the DSM with Latin Hypercube Sampling (LHS), called Explorative Gradient Method (EGM). Although the optimization routines are all model-free, by exploiting our knowledge of the thermoacoustic model we also analyzed the behaviour of the thermoacoustic system in frequency domain. This enabled us to emphasize differences between frequency and time domain analysis. By examining three case-studies with increasing level of complexity, we identified and discussed advantages and disadvantages of the different optimization routines. While DSM efficiently identifies local minima, it does not find the global minimum when initialized near a local minimum. The EA is able to identify the global minimum for the presented cases, but required more function evaluations, and thus generates higher computational costs. The EGM

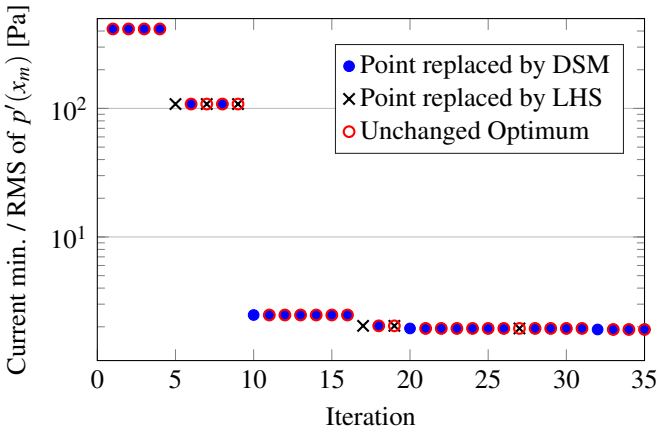

FIGURE 7. Optimization run for Case III with 5 fuel injectors. The current minimum in each iteration is illustrated and the underlying subroutine for each iteration is indicated by different markers.

optimizer is more robust compared to DSM and found the global minimum even when initialized close to the local minimum. The LHS steps performed by the EGM allow for a uniform exploration of the objective function, whereas the EA explores the parameter space based on information of previously evaluated points via crossovers and mutations. For the chosen convergence criteria, the EGM algorithm always requires less function evaluations than the EA to find the minimum in the analyzed cases. Notably, we observed that time domain optimization based on the saturated oscillation amplitudes and frequency domain analysis based on the linear stability may yield different optimal conditions. This is because, in general, a larger growth rate does not imply a larger oscillation amplitude. This is particularly true when more than one mode is thermoacoustically linearly unstable, as there is no guarantee that the mode with the largest growth rate will dominate the dynamics.

Lastly, we discussed how, since thermoacoustic systems can feature multiple unstable modes simultaneously, the objective functions can generally have complex shapes and exhibit several local minima. Moreover, since bi-stability has been observed in thermoacoustics, the initial conditions may affect the nonlinear saturation and the oscillation amplitude, making the problem even more complex. These phenomena place great demand on the optimization routines. As a matter of fact, the performance of an optimization method depends on the problem that one wishes to optimize. For all the cases considered here, the EGM optimization algorithm shows the best convergence properties and can, to a certain extend, be considered the most effective method of the analyzed ones to solve problems of such nature. However, this may not be true if the objective function is changed, and no general conclusions on the best choice of an optimization routines for thermoacoustic systems can be drawn.

The results of this work show that gradient-free optimization in time domain is a promising tool for the optimization of thermoacoustic systems and yields more robust results than eigenvalue-based analysis. Together with recent advances in the field of optimization, which show a significant increase of convergence speed, these results suggest that optimization routines may be of interest also for the optimization of experimental combustion systems that may exhibit thermoacoustic oscillations. However, this study also revealed that thermoacoustic problems place great demands on the optimization routines. This is expected to be even more true when more complex application-related tasks with multi-valued objective functions – such as the simultaneous optimization of emissions and pulsations – are addressed.

ACKNOWLEDGMENT

J. M. Reumschüssel and J. G. R. von Saldern acknowledge the German Ministry of Economy and Technology and MAN Energy Solutions SE for funding within the scope of the AG Turbo project ROBOFLEX (grant nr. 03EE5013E). A. Orchini acknowledges funding from the DFG (project nr. 422037803). The authors would like to thank Jan-Peter Hannappel for his help with the evolutionary algorithm and Dr. Bernhard Ćosić for helpful discussions in the early phase of the project.

REFERENCES

[1] Lieuwen, T., 2012. *Unsteady combustor physics*. Cambridge University Press.

[2] Candel, S., 2002. "Combustion Dynamics and Control: Progress and Challenges". *Proceedings of the Combustion Institute,* ***29***, pp. 1–28.

[3] Mongia, H. C., Held, T. J., Hsiao, G. C., and Pandalai, R. P., 2003. "Challenges and Progress in Controlling Dynamics in Gas Turbine Combustors". *Journal of Propulsion and Power,* ***19***, pp. 822–829.

[4] Moeck, J. P., Lacarelle, A., and Paschereit, C. O., 2008. "Subcritical thermoacoustic instabilities in a premixed combustor". *Proceedings of the 29th AIAA Aeroacoustics Conference,* ***2946***, p. 18 pages.

[5] Dowling, A. P., 1995. "The calculation of thermoacoustic oscillations". *Journal of Sound and Vibration,* ***180***, pp. 557–581.

[6] Polifke, W., 2010. "Low-Order Analysis Tools for Aero- and Thermo-Acoustic Instabilities". In *Advances in Aero-Acoustics and Thermo-Acoustics*. Van Karman Institute for Fluid Dynamics, p. 59.

[7] von Saldern, J. G. R., Moeck, J. P., and Orchini, A., 2020. "Nonlinear interaction between clustered unstable thermoacoustic modes in can-annular combustors". *Proceedings of the Combustion Institute,* ***In Press***.

[8] Noiray, N., and Schuermans, B., 2012. "Theoretical and experimental investigations on damper performance for suppression of thermoacoustic oscillations". *Journal of Sound and Vibration,* ***331***, pp. 2753–2763.

[9] Aguilar, J. G., and Juniper, M. P., 2018. "Adjoint methods for elimination of thermoacoustic oscillations in a model annular combustor via small geometry modifications". *Proceedings of the ASME Turbo Expo,* ***2018***, pp. 1–11.

[10] Büche, D., Stoll, P., Dornberger, R., and Koumoutsakos, P., 2002. "Multiobjective evolutionary algorithm for the optimization of noisy combustion processes". *IEEE Transactions on Systems, Man and Cybernetics Part C: Applications and Reviews,* ***32***(4), pp. 460–473.

[11] Paschereit, C. O., Schuermans, B., and Büche, D., 2003. "Combustion Process Optimization Using Evolutionary Algorithm". *Proceedings of the ASME Turbo Expo,* ***2003***, pp. 281–291.

[12] Hansen, N., Niederberger, A., Guzzella, L., and Koumoutsakos, P., 2006. "Evolutionary Optimization of Feedback

Controllers for Thermoacoustic Instabilities". *IUTAM Symposium on Flow Control and MEMS,* ***Sep 2006***.

[13] Janiga, G., and Thévenin, D., 2007. "Reducing the CO emissions in a laminar burner using different numerical optimization methods". *Proceedings of the Institution of Mechanical Engineers, Part A: Journal of Power and Energy,* ***221***(5), pp. 647–655.

[14] Faramarzi, A., Heidarinejad, M., Stephens, B., and Mirjalili, S., 2020. "Equilibrium optimizer: A novel optimization algorithm". *Knowledge-Based Systems,* ***191***, p. 105190.

[15] Nelder, J. A., and Mead, R., 1965. "A simplex method for function minimization". *The computer journal,* ***7***, pp. 308–313.

[16] Hilgers, A., and Boersma, B. J., 2001. "Optimization of Jet Mixing". *Fluid Dynamics Research,* ***29***, pp. 345–368.

[17] Li, R., Noack, B. R., Cordier, L., Borée, J., and Harambat, F., 2017. "Drag reduction of a car model by linear genetic programming control". *Experiments in Fluids,* ***58***, pp. 1–20.

[18] Brunton, S. L., and Noack, B. R., 2015. "Closed-loop turbulence control: Progress and challenges". *Applied Mechanics Reviews,* ***67***, p. 050801 (48 pages).

[19] Li, Y., Cui, W., Jia, Q., Li, Q., Yang, Z., Morzynski, M., and Noack, B. R., 2020. "Explorative gradient method for active drag reduction of the fluidic pinball and slanted Ahmed body". *Submitted to the Journal of Fluid Mechanics*.

[20] Polifke, W., and Lawn, C., 2007. "On the low-frequency limit of flame transfer functions". *Combustion and Flame,* ***151***, pp. 437–451.

[21] Orchini, A., Illingworth, S., and Juniper, M., 2015. "Frequency domain and time domain analysis of thermoacoustic oscillations with wave-based acoustics". *Journal of Fluid Mechanics,* ***775***, p. 387–414.

[22] Gustavsen, B., and Semlyen, A., 1999. "Rational approximation of Frequency Domain Responses by Vector Fitting". *IEEE Transactions on Power Delivery,* ***14***, pp. 1052–1061.

[23] Abu-Orf, G. M., and Cant, R. S., 1996. "Reaction rate modelling for premixed turbulent methane-air flames". *Proceedings of the Joint Meeting of the Portuguese, British and Swedish Sections of the Combustion Institute,* ***1996***, p. 4 pages.

[24] Kawanabe, H., Shioji, M., Tsunooka, T., Ali, Y., 1998. "CFD Simulation for Predicting Combustion and Pollutant Formation in a Homogenuous Charged SI Engine". *The Fourth International Symposium COMODIA,* ***C98***, pp. 233–238.

[25] Lieuwen, T., 2003. "Modeling Premixed Combustion-Acoustic Wave Interactions: A Review". *Journal of Propulsion and Power,* ***19***, pp. 765–781.

[26] Schuller, T., Durox, D., and Candel, S., 2003. "A unified model for the prediction of laminar flame transfer functions: comparisons between conical and V-flames dynamics". *Combustion and Flame,* ***134***, pp. 21–34.

[27] Rigas, G., Jamieson, N. P., Li, L. K., and Juniper, M. P., 2015. "Experimental sensitivity analysis and control of thermoacoustic systems". *Journal of Fluid Mechanics,* ***787***, pp. 1–11.

[28] McKay, M. D., Beckman, R. J., and Conover, W. J., 2000. "A comparison of three methods for selecting values of input variables in the analysis of output from a computer code". *Technometrics,* ***42***, pp. 55–61.

[29] Wahde, M., 2008. *Biologically inspired optimization methods: an introduction*. WIT Press.

[30] Bäck, T., and Schwefel, H.-P., 1993. "An Overview of Evolutionary Algorithms for Parameter Optimization". *Evolutionary Computation,* ***1***, pp. 1–23.

[31] Trautmann, H., Wagner, T., Naujoks, B., Preuss, M., and Mehnen, J., 2009. "Statistical methods for convergence detection of multi-objective evolutionary algorithms". *Evolutionary Computation,* ***17***, pp. 493–509.

[32] Humbert, S. C., Gensini, F., Andreini, A., Paschereit, C. O., and Orchini, A., 2020. "Nonlinear analysis of self-sustained oscillations in an annular combustor model with electroacoustic feedback". *Proceedings of the Combustion Institute,* ***In Press***.

A Parameter values

Model parameters. The values used for modelling the flame speed are taken from the literature for methane-air combustion at atmospheric conditions and are stated in Tab.2. The geometric and mean flow parameters that were used in all cases are summarized in Tab. 3. Case-specific values of boundary and geometric parameters are shown in Tab. 4.

Optimization parameters. For the stopping criterion of the EGM and DSM algorithm, $\delta = 0.05$ was used. The convergence of the evolutionary algorithm was tested with a χ^2 test, requiring 95% of statistical significance for a variance of 5% over the last 7 generations for convergence.

TABLE 2. Parameters for flame model [23, 24].

C [-]	V [$\frac{\text{m}}{\text{s}}$]	n [-]	a [$\frac{\text{m}}{\text{s}}$]	b [-]	c [-]	d [-]
1.25	0.2	0.7	0.6097	-2.554	7.31	1.23

TABLE 3. Geometric and mean flow parameters used in the study.

A_c [m^2]	L [m]	T_1 [K]	p_1 [bar]	u_1 [$\frac{\text{m}}{\text{s}}$]	Γ [$\frac{\text{m}^2}{\text{s}}$]	x_m [m]
$\pi\,(0.05)^2$	1	350	1	8	0.001	0.99

TABLE 4. Geometric and boundary parameters for different cases.

Case	Param.	R_1	R_2	x_f	x_1	x_2	x_3	x_4	x_5
	Unit	-	-	m	m	m	m	m	m
I.		-1	0.75	0.2	0.05	0.15			
II.		-1	0.9	0.3	0.2	0.225	0.25		
III		-1	0.9	0.3	0.2	0.21	0.225	0.24	0.25